# Validation of JENDL-3.3 for the HTTR Criticality

Minoru GOTO, Naoki NOJIRI and Satoshi SHIMAKAWA
*Department of HTTR Project, Japan Atomic Energy Research Institute*
*3607 Oarai-machi, Higashi-ibaraki-gun, Ibaraki-ken 311-1394*
e-mail: mgotoh@oarai.jaeri.go.jp

Validation of JENDL-3.3 has been performed for the HTTR criticality using the MVP code with a "lattice-cell" of infinite models and a "whole-core" of finite models. It was found that the *keff* values calculated with JENDL-3.3 was decreased about 0.2-0.4%$\Delta k$ from one with JENDL-3.2. The criticality prediction was closed to the experimental data in the critical approach situation of the HTTR.

## 1. Introduction

Benchmark calculations for several water-moderated reactors had been performed with JENDL-3.3 which is the latest version of the Japan Evaluated Nuclear Data Library (JENDL) and the *keff* values are obtained good agreements with the experimental data rather than JENDL-3.2 which is the previous version of JENDL[1].

Concerning to high temperature gas-cooled reactors, obtaining good calculation results with JENDL-3.3 are expected as mentioned above, too. To improve the HTTR core calculations with high accuracy, the JENDL-3.3 has been attempted in this study.

This report describes the applicability of JENDL-3.3 to the HTTR criticality and the comparisons between the calculation results with JENDL-3.2 and the experimental data.

## 2. General descriptions of the HTTR

### 2.1 Core structure

The HTTR is a graphite-moderated, helium-cooled thermal reactor which has 30MW of thermal power and 950℃ of outlet coolant-gas temperature. Radial and axial views of the HTTR are shown in Fig.1. The center of the core is constructed with fuel assembly blocks with different 12 kinds of enrichment (3.4-9.9wt-%U), control rod guide blocks, reflector blocks and irradiation blocks, and is surrounded by the permanent reflector. There are two types of the fuel assembly blocks with 33 and 31 fuel rods which composed 14 fuel compacts. Each fuel compact composes about 13,000 coated fuel particles of 0.92mm diameter.

### 2.2 Critical approach

The critical approach of the HTTR was carried out by the fuel addition method at room temperature. In this situation, the dummy graphite blocks were replaced to the flesh fuel blocks from outer core region and then the annular core was made with 18 fuel columns. Each fuel column consists of five fuel blocks. The initial critical state was achieved with 19 fuel columns and the full core with 30 fuel columns, i.e. 150 fuel brocks, was successfully constructed.

## 3. Calculation methods

Calculations for the HTTR criticality were performed by the continuous energy Monte Carlo code MVP[2] with the neutron cross section sets based on JENDL-3.3 and JENDL-3.2. In the calculations, there were two different geometrical models which were "whole-core" and "lattice-cell" for following issues.

(1) the discrepancy between the calculated *keff* value and the experimental data of the critical approach

(2) the contribution of each nuclide data on the *keff* discrepancy between JENDL-3.3 and JENDL-3.2

(3) the major cause of the *kinf* discrepancy on temperature dependency

The calculation conditions are shown in Table1. The first two issues were performed with the "whole-core" model, and the last issue was performed with the "lattice-cell" model. The standard deviations of the calculation results with the "whole-core" model and the "lattice-cell" model were less than 0.03% and 0.01%, respectively. The history numbers of the each calculation were 8,000,000.

## 4. Calculation results and discussions

### 4.1 Critical approach

Calculated *keff* values for the critical approach are shown in Fig.2 and the initial critical state would be achieved by 18 fuel columns loaded. In the experiment that was achieved by 19 fuel columns loaded. The *keff* line with JENDL-3.3 is under the one with JENDL-3.2 and its discrepancy is 0.2-0.4%$\Delta k$, therefore JENDL-3.3 gives slightly better *keff* value rather than JENDL-3.2. However, an overestimation to the experimental data about 0.8%$\Delta k$ is remained.

### 4.2 Nuclide contributions to the critical calculations

The *keff* discrepancy caused by the difference of JENDL's version and the contributions of the differences of each nuclide data to the discrepancies were shown in Fig.3. For 18 and 30 fuel columns loaded cores, JENDL-3.3 gives 0.30 and 0.40%$\Delta k$ smaller *keff* value than JENDL-3.2, respectively. Here, the U-235 data of JENDL-3.3 gives 0.35 and 0.45%$\Delta k$ smaller *keff* value than one of JENDL-3.2. The *keff* discrepancy caused by the difference of another nuclide data was less than 0.10%$\Delta k$. As the results, the discrepancy caused by the difference of JENDL's version is dominated by the difference of the U-235 data.

In order to treat $S(\alpha,\beta)$ data, the MVP neutron cross section sets based on JENDL-3.3 and JENDL-3.2 were taken it form ENDF/B-VI and ENDF/B-III, respectively. With the improvement from ENDF/B-III to ENDF/B-VI, upper energy limitation of the $S(\alpha,\beta)$ data of Graphite was extended. However, it was confirmed that the influence of this difference on the *kinf* values is negligible.

### 4.3 *kinf* and *keff* values with JENDL-3.3

The ratios of the *kinf* or the *keff* values with JENDL-3.3 to JENDL-3.2 for the HTTR at high and room temperature conditions and the water-moderated reactors at room temperature were plotted by uranium enrichment in Fig.4[1]. There is a difference between the distribution pattern of the ratios for all reactors at room temperature and the HTTR at high temperature.

To reveal the reason of the difference in the distribution pattern mentioned above, the temperature dependencies of the ratio of the HTTR *kinf* values were examined. As shown in Fig.5, the ratios decreased according with the rise of temperature.

Furthermore, to examine the temperature dependency of the *kinf* values in detail, the analysis was performed by using the four-factor formula. Each of the factors is defined following equations and each of their right hand factors which means reaction rate can be obtained directly from the MVP calculations[3].

$$\varepsilon = \frac{[\nu \cdot \Sigma_f \cdot \phi \cdot V]_{fast}^{fuel} + [\nu \cdot \Sigma_f \cdot \phi \cdot V]_{thermal}^{fuel}}{[\nu \cdot \Sigma_f \cdot \phi \cdot V]_{fast}^{fuel}} \qquad (1)$$

$$p = \frac{[\Sigma_a \cdot \phi \cdot V]_{thermal}^{whole}}{[\Sigma_a \cdot \phi \cdot V]_{fast}^{whole} + [\Sigma_a \cdot \phi \cdot V]_{thermal}^{whole}} \qquad (2)$$

$$f = \frac{[\Sigma_a \cdot \phi \cdot V]_{thermal}^{fuel}}{[\Sigma_a \cdot \phi \cdot V]_{termal}^{whole}} \qquad (3)$$

$$\eta = \frac{[\nu \cdot \Sigma_f \cdot \phi \cdot V]_{thermal}^{fuel}}{[\Sigma_a \cdot \phi \cdot V]_{thermal}^{fuel}} \qquad (4)$$

where,

$\varepsilon$: first fission factor, p: resonance escape probability,
f: thermal utilization, $\eta$: thermal regeneration rate,
$\nu$: number of neutrons per fission, $\Sigma$: macroscopic cross section,
$\phi$: flux and V: volume.

In the equations, the neutron energy range was divided into the thermal and the fast range with a boundary value 4.5eV. From Fig.6, the discrepancy between the *kinf* values with JENDL-3.3 and JENDL-3.2 at room temperature was dominated by discrepancy of the p and $\eta$ values. The temperature dependency of the *kinf* values was dominated only by the $\eta$ values discrepancy. By considering the nuclide contributions to each reaction rate in the equation (2) and (4), it was found that the discrepancies of the p and $\eta$ values mentioned above were caused mainly by the difference of the U-235 fission data.

The ratios of the $\eta$ values with JENDL-3.3 to JENDL-3.2 and the neutron spectra at 300K and 1200K are plotted by neutron energy in Fig.7. In the equation (4), the $\nu$ value is approximately constant and $\Sigma_a^{U235} >> \Sigma_a^{U238}$, therefore the $\eta$ values are in proportion to the ratio of microscopic fission cross section data of U-235 to microscopic absorption cross section data of U-235. Figure7 suggests that the neutron spectrum is shifted to the right by the rise of temperature and this shift causes decreasing the $\eta$ values ratio. This effect makes the discrepancy of the *kinf* values increase. This will be an important for the calculations of the temperature coefficients at high temperature.

## 5. Summary

For the HTTR criticality analysis, the calculations by the MVP code with JENDL-3.3 provides some improvements as follows,

For room temperature conditions;

(1) JENDL-3.3 gives 0.4%$\Delta k$ better *keff* value than JENDL-3.2 and 0.8%$\Delta k$ overestimation to the experimental data, however, is remained.

(2) Discrepancies between the *keff* values with JENDL-3.3 and JENDL-3.2 are

caused mainly by the difference of the p and η values of the U-235 data.

For high temperature conditions;

(3) Discrepancies between the *kinf* values with JENDL-3.3 and JENDL-3.2 become large according with the rise of temperature.

(4) This is because that the magnitude of the temperature dependency of the *kinf* values with JENDL-3.3 is grater than one with JENDL-3.2 and

(5) it is caused by the difference between the η values with JENDL-3.3 and JENDL-3.2 in thermal energy range.

The calculations with JENDL-3.3 will be employed successfully in the future works.

## References


[1] K. Okumura and T. Mori: JAERI-Review 2003-023, p.59

[2] T. Mori and M. Nakagawa: JAERI-Data/Code 94-007

[3] K. Okumura: Private communications


Table 1 Calculation conditions

| System temperature | Calculation model | Critical index | Comparative data | History number | Standard deviation (1σ) |
|---|---|---|---|---|---|
| 300, 600, 900 and 1200K | lattice-cell with STG** | *kinf* | Calc. with J32*** | 8,000,000 | < 0.01% |
| 300K, ~1200K* | whole-core with STG | *keff* | Calc. with J32 and Exp. data (300K) | 8,000,000 | < 0.03% |

* at FULL power condition
** statistical geometry
*** JENDL-3.2

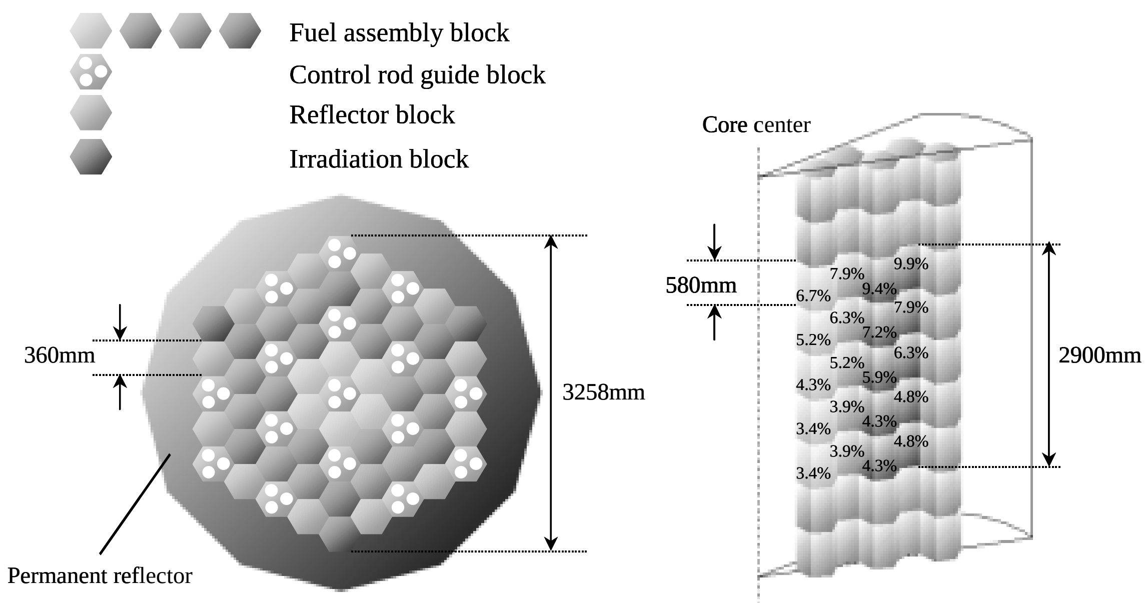


Radial view of the HTTR core

Axial view of the HTTR core and arrangement of fuel enrichment

Fig.1 Radial and axial view of the HTTR core and arrangement of fuel enrichment

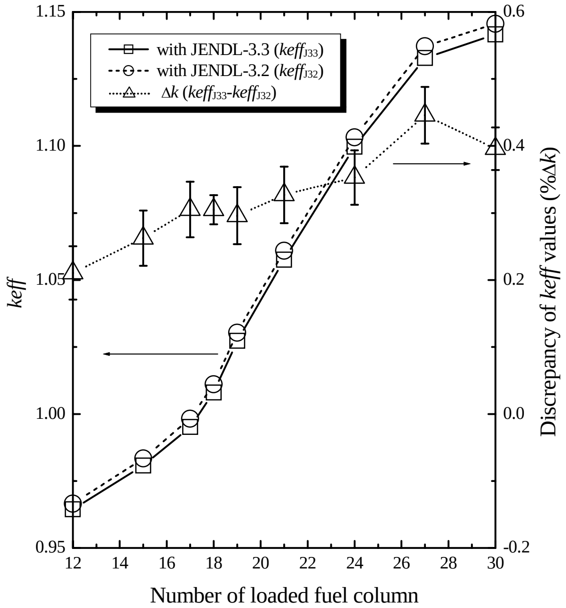


Fig.2 Calculated *keff* values for the critical approach

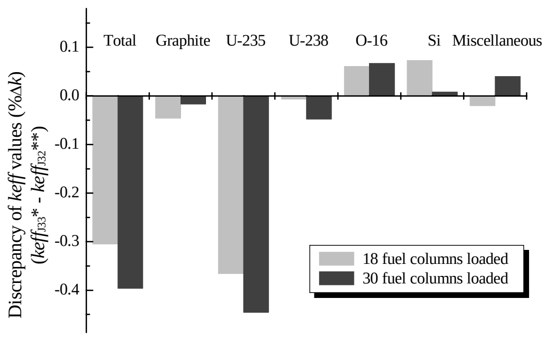


Fig.3 Contributions of the nuclide data to the *keff* values

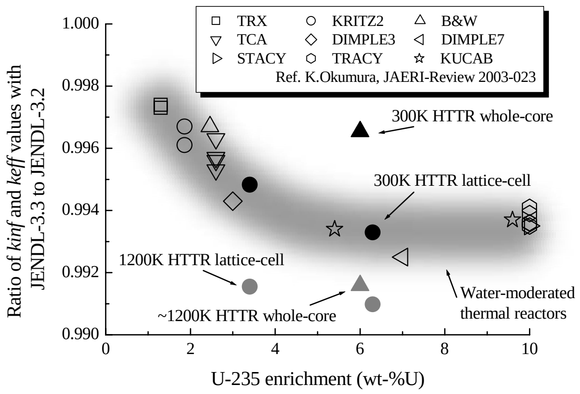


Fig.4 Distributions of the ratios of the *kinf* and *keff* values

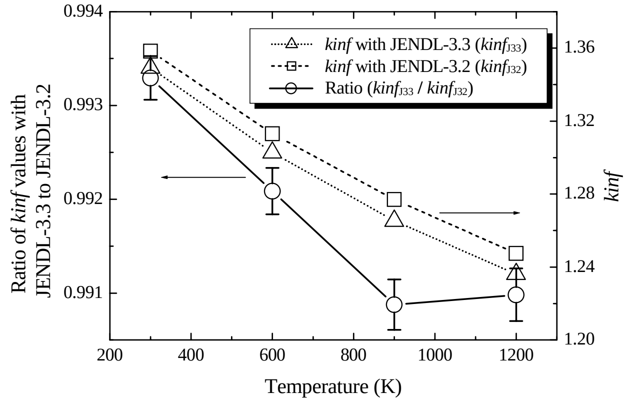


Fig.5 Temperature dependency of the ratios of the *kinf* values

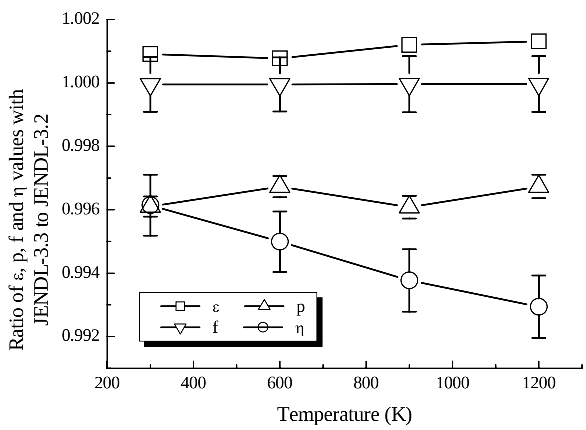


Fig.6 Temperature dependency of the ratio of the four factors

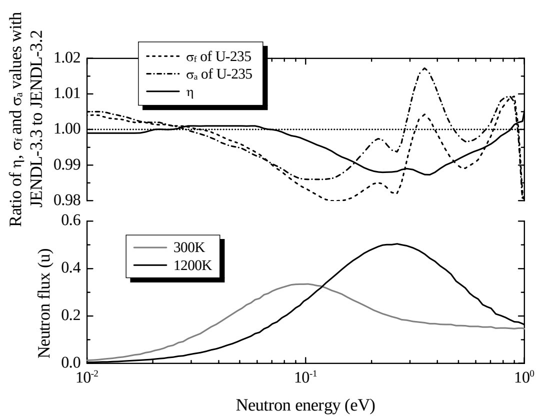


Fig.7 Ratios of the η values and the neutron spectra at 300 and 1200K